Supporting Information for the Manuscript

Thermally-Induced Structural Evolution of Silicon- and Oxygen-Containing Hydrogenated Amorphous Carbon: A Combined Spectroscopic and Molecular Dynamics Simulation Investigation

Filippo Mangolini[1], James Hilbert[2], J. Brandon McClimon[3], Jennifer R. Lukes[2], and Robert W. Carpick[2,*]

[1] Materials Science and Engineering Program and Department of Mechanical Engineering, The University of Texas at Austin, Austin, Texas 78712, USA
[2] Department of Mechanical Engineering and Applied Mechanics, University of Pennsylvania, Philadelphia, Pennsylvania 19104, USA
[3] Department of Materials Science and Engineering, University of Pennsylvania, Philadelphia, Pennsylvania 19104, USA

* To whom correspondence should be addressed:
Professor Robert W. Carpick
Department of Mechanical Engineering and Applied Mechanics,
University of Pennsylvania
229 Towne Bldg., 220 S. 33rd Street
19104-6315 Philadelphia, PA, USA

Phone: +1-215-898-4608
Fax: +1-215-573-6334
carpick@seas.upenn.edu

Experimental

Materials

Silicon- and oxygen-containing hydrogenated amorphous carbon (a-C:H:Si:O) coatings were deposited on silicon wafers by Sulzer-Metco Inc. (Amherst, NY, USA) using a proprietary plasma-enhanced chemical vapor deposition (PECVD) process, whose details are described elsewhere[1-9]. Briefly, a plasma discharge was formed from a proprietary siloxane precursor by means of a hot filament, whose temperature ranged between 2073 K and 2273 K. During the deposition, a negative radio frequency (RF) bias voltage between -300 and -500 V was applied to the substrate. Although the substrate temperature was not deliberately increased during the deposition process, it could locally increase due to ion impingement on the surface; the temperature rise is expected to be no more than 200 degrees above room temperature. The thickness of the a-C:H:Si:O coating was 2 μm. A detailed description of the characterization of the bulk chemistry and structure of the as-received coatings is reported in Ref. 10. The chemical composition of the films was: [C] = 57±3 at.%; [O] = 3±1 at.%; [Si] = 6±1 at.%; [H] = 34±3 at.% (measured by Rutherford backscattering spectrometry and hydrogen forward scattering spectrometry, Evans Analytical Group, Sunnyvale, CA, USA)[9-10]. The film density, determined by X-ray reflectivity, was 1.8±0.1 g/cm^3 [9-10]. The comparison between XPS (the information depth for electrons with kinetic energy equal to 1383 eV travelling in a-C:H:Si:O: 9.5 nm [11]) and RBS/HFS (bulk sensitive) results indicated a good agreement between [C]/[Si] ratios, while a higher [O]/[Si] ratio in the case of XPS data, thus suggesting the presence of an oxidized near-surface layer in a-C:H:Si:O.

Hydrogen-terminated ultrananocrystalline diamond (UNCD Aqua 25, Advanced Diamond Technologies, Romeoville, IL, USA) and freshly cleaved highly ordered pyrolytic graphite (HOPG, grade 2, SPI Supplies, West Chester, PA, USA) were used as reference compounds for near edge X-ray absorption fine structure (NEXAFS) spectroscopic measurements.

Methods

X-Ray Photoelectron Spectroscopy (XPS)

The chemistry of the near-surface region of silicon- and oxygen-containing hydrogenated amorphous carbon (a-C:H:Si:O) was investigated by X-ray photoelectron spectroscopy (XPS) using a customized XPS spectrometer, extensively described in Ref. 12. Briefly, the XP-spectrometer is equipped with a monochromatic Al Kα X-ray source with a beam diameter of 1 x 3 mm^2. The photoelectrons emitted from the specimen are collected with an electrostatic lens, whose axis is normal to the sample surface. After passing the hemispherical analyzer, the photoelectrons are detected by a two-dimensional MCP/CCD detector.

In the present work, the X-ray source was run at 30 mA and 12 kV, whereas the analyzer was operated in constant-analyzer-energy (CAE) mode. Survey spectra were acquired with the pass energy and step size equal to 200 eV and 1 eV, respectively. For the high-resolution (HR) spectra, the pass energy and step size were, respectively, 100 and 0.05 eV (full width at half maximum (FWHM) of the peak height for the Ag $3d_{5/2}$ equal to 0.57 eV). The curved slit at the entrance of the hemispherical analyzer has a width of 0.8 mm. The residual pressure in the analysis chamber was always below 1 x 10^{-6} Pa. The spectrometer was calibrated according to ISO 15472:2001 with an accuracy better than ±0.05 eV. The high-resolution spectra were processed using CasaXPS software (v2.3.16, Casa Software Ltd., Wilmslow, Cheshire, U.K.). An iterated Shirley-Sherwood background subtraction was applied before peak fitting using a linear least-square algorithm[13]. No sample charging was ever observed, as determined by checking the position of the carbon (C 1s) signal and of the valence band (this is expected since the samples have moderate electrical conductivity). The high-resolution Si

2p spectra of a-C:H:Si:O (Figure 1c) were the convolution of the $2p_{3/2}$ and $2p_{1/2}$ components due to spin-orbit splitting. Curve synthesis was performed constraining the integrated intensity ratio of these two signals to 0.5 and their separation to 0.65 eV. In Figure 1c, the $2p_{3/2}$ and $2p_{1/2}$ components for each chemical state were summed up into a single envelope for clarity.

The quantitative evaluation of XPS data, as described in Ref. 14-15, was based on the integrated intensity (*i.e.*, the peak area in Cps x eV obtained from the original spectra after background subtraction and curve synthesis) using a first principles model and applying Powell's equations[16]. The inelastic mean free path (the mean distance traveled by electrons with a given kinetic energy (KE) between inelastic collisions in the material[17]) was calculated using the TPP-2M formula[18].

Since the as-received a-C:H:Si:O samples exhibited a multilayer structure (*i.e.*, a 2 μm-thick a-C:H:Si:O coating covered by a carbonaceous contamination layer due to sample exposure to air), a multilayer model was applied to estimate the composition of each layer and the thickness of the contamination layer. The equations that correlate the integrated intensity and the concentration of the emitting element were taken from the work of Seah[19] and Fadley[20], assuming the electrons emitted from each layer to be attenuated by the layer itself and the overlayer (according to the Beer-Lambert law). In the present work, each layer is assumed to be homogeneous in thickness and composition. Furthermore, it is assumed that carbon-oxygen bonds are only present in the contamination layer. Under this assumption, the composition calculated by XPS more closely agrees with the results of secondary ion mass spectrometry (SIMS) and Rutherford backscattering spectrometry (RBS) (SIMS and RBS measurements were performed by Evans Analytical Group, Sunnyvale, CA, USA). The system of non-linear equations was numerically solved using Mathematica (v9.0, Wolfram Research, Champaign, IL, USA), thus enabling the computation of the thickness and composition of each layer constituting the multilayer structure.

To investigate the structural evolution of a-C:H:Si:O *vs.* temperature, heating experiments were performed inside the XPS chamber under high vacuum conditions. The samples (6 x 6 mm^2) were mounted in a holder (RHK Technology, Inc., Troy, MI, USA) that included a tungsten filament for radiative heating and a K-type thermocouple in contact with the sample for recording specimen temperature. The films were annealed in progressive steps from 150°C to 500°C at 50°C intervals for 1 h and cooled after each anneal (heating and cooling rate: 10°C/min). The XPS spectra, whose acquisition required approximately 9 h, were collected after cooling the sample to below 40°C after each heating step.

All the XPS results reported here are mean values calculated from at least three independent measurements, with the corresponding standard deviation reported.

Near Edge X-Ray Absorption Fine Structure (NEXAFS) Spectroscopy

Near edge X-ray absorption fine structure (NEXAFS) spectroscopic measurements were performed at the NIST/Dow endstation of beamline U7A and at the Oak Ridge National Laboratory endstation of beamline U12A at the National Synchrotron Light Source (NSLS), Brookhaven National Laboratory (Upton, NY, USA). The photon source of these beamlines is a bending magnet, and covers an energy range from 180 to 1100 eV for U7A and from 100 to 800 eV for U12A. The photon flux is $2x10^{11}$ photons/second/0.1% bandwidth, and the resolution ($\Delta E/E$) is ~1 x 10^{-3}. All measurements were carried out in partial electron yield (PEY) mode and at a photon incidence angle of 55° with respect to the sample surface (the so-called "magic angle") to suppress the effects related to the X-ray polarization[21]. For the experiments described here, the entrance grid bias (EGB) of the channeltron detector was set to -225 V at U7A and to -230 V at U12A to enhance surface sensitivity and minimize the detection of Auger electrons that suffered from energy loss while travelling through the sample before being emitted into the continuum. The monochromator energy was calibrated using the carbon $1s \rightarrow \pi^*$

transition of freshly-cleaved highly ordered pyrolytic graphite (HOPG, grade 2, SPI Supplies, West Chester, PA, USA), located at 285.5 eV. The spectra acquired at U7A were first normalized to the absorption current measured simultaneously from a gold mesh placed in the beamline upstream from the analysis chamber. The spectra acquired at U12A were first normalized to the absorption current measured under the same experimental conditions on a sputter-cleaned platinum sample. After this pre-edge normalization, the spectra were normalized based on the absorption intensity in the post-edge (continuum) region (at 320 eV). In this way, variations in spectral intensity only arise from chemical changes and are independent of the number density of absorbing atoms. Since the analyses carried out at U7A and at U12A provided comparable results, only the spectra acquired at the former beamline are displayed in the present work.

Since the a-C:H:Si:O samples under investigation were exposed to air before the NEXAFS analyses, the as-acquired C 1s NEXAFS spectra are a convolution of the spectrum of a-C:H:Si:O and the spectrum of the adventitious carbon contamination on the a-C:H:Si:O surface since the thickness of the latter (<1 nm, calculated from XPS data) is smaller than the information depth at the carbon 1s (usually less than 5 nm [21]). To remove the contribution of the carbonaceous contamination layer from the as-acquired C 1s NEXAFS spectra, the method outlined in Ref. 22 was applied. The method relies on the subtraction of the NEXAFS spectrum of the carbonaceous contamination layer adsorbed on a reference surface (*i.e.*, gold) from the as-acquired spectrum of the air-exposed sample under investigation (*i.e.*, a-C:H:Si:O), where the thickness of the contamination layer is independently determined by XPS. The removal of the contribution of the contamination layer from the as-acquired NEXAFS spectra allowed the intrinsic photo-absorption NEXAFS spectra of a-C:H:Si:O to be computed.

The quantitative evaluation of the fraction of sp^2-bonded carbon in the specimens on the basis of NEXAFS data (corrected for the contribution of the contamination layer) was performed using the procedure described in Ref. 23. The method is based on the relative integrated intensity ratios of the C 1s$\rightarrow\pi^*$ and C 1s$\rightarrow\sigma^*$ peaks for the sample under investigation and for a reference specimen:

$$f_{sp^2} = \frac{I_{sam}^{\pi^*} I_{ref}\left(\Delta E\right)}{I_{sam}\left(\Delta E\right) I_{ref}^{\pi^*}} \qquad \text{Eq. 1}$$

where $I_{sam}^{\pi^*}$ and $I_{ref}^{\pi^*}$ are, respectively, the areas of the C 1s$\rightarrow\pi^*$ peaks for the sample and the reference, whereas $I_{sam}\left(\Delta E\right)$ and $I_{ref}\left(\Delta E\right)$ are the areas under the NEXAFS spectrum between 288.6 eV and 320 eV for the sample and the reference, respectively. As a reference, the spectrum of freshly-cleaved HOPG (100% sp^2-bonded carbon) sample was acquired with the X-ray beam incident at an angle of 40° to the sample surface to account for the $\cos^2(\Theta)$ (Θ angle between the X-ray beam and the sample surface) angular dependence of the π^* and σ^* resonance intensity[21] and for the polarization factor of the impinging X-rays[23].

To investigate the structural evolution of a-C:H:Si:O *vs.* temperature, heating experiments were performed inside the NEXAFS endstation chamber under high vacuum conditions. The samples (~8 x 8 mm^2) were mounted on a custom-made holder that included a tungsten filament for heating and a K-type thermocouple in contact with the sample for recording specimen temperature. The films were annealed in progressive steps from 150°C to 450°C at 100°C intervals for 1 h. Since the acquisition of NEXAFS data only required 5 min, the spectra were collected without cooling the sample to room temperature (*i.e.*, they were acquired at elevated temperature).

All the NEXAFS results reported here are mean values calculated from at least three independent measurements, with the corresponding standard deviation reported.

Molecular Dynamics (MD) Simulations

Molecular dynamics (MD) simulations were performed using the ReaxFF potential[24-28]. This empirical bond order potential, which allows chemical reactions to take place and be investigated, can be used to simulate any combination of elements, provided an appropriate set of fitting parameters has been found. These fitting parameters are derived from either experimental data or quantum mechanical simulations. For simulating a-C:H:Si:O, the Si/C/H/O force field developed by Newsome *et. al.* was used[26]. The simulations were carried out using the molecular dynamics program LAMMPS (Sandia National Laboratories, http://lammps.sandia.gov)[29-30].

The amorphous structure of a-C:H:Si:O was produced in MD simulations by liquid quenching, which is a computationally efficient method to produce amorphous carbon samples in MD simulations. It has been shown by Li *et al.*[31] that the ReaxFF potential can reproduce experimentally-observed properties of amorphous carbon through liquid quenching, and a physical basis for the liquid quenching procedure was provided by Marks[32]. The initial simulation cell consisted of 2744 atoms selected to match the experimental atomic composition ([C] = 57±3 at.%; [O] = 3±1 at.%; [Si] = 6±1 at.%; [H] = 34±3 at.%, measured by Rutherford backscattering spectrometry and hydrogen forward scattering spectrometry, Evans Analytical Group, Sunnyvale, CA, USA) at a density of 2.3 g/cm^3. Periodic boundary conditions were used in x, y, and z directions and the simulations were carried out in the NVE ensemble. The temperature was increased by velocity rescaling to 6,000 K, which was observed to be sufficient to melt the initial structure, and was maintained for 3 ps. The temperature was then reduced to 300 K over 1 ps, and the resulting structure was equilibrated. It has been shown previously that short quenching times, on the order of 1 ps or less, are capable of producing accurate amorphous carbon structures[33-34], and analysis of film deposition experiments has shown sub-picosecond thermal spikes are produced by energetic ions impacting the surface, providing a theoretical basis for the liquid quenching timescale[32]. The simulated a-C:H:Si:O structure was then further relaxed in an NPT ensemble with a Nose-Hoover thermostat and barostat to 300 K and no external pressure. This reduced the density to 1.92 g/cm^3. Finally, the periodic boundary conditions in $\pm y$ were removed to form free surfaces, which were relaxed over 5 ps. The liquid quenching procedure resulted in a final a-C:H:Si:O structure which is shown in Figure S.1. For comparison, a simulated a-C:H sample was also produced using the same liquid quenching procedure. The simulated a-C:H sample consisted of 2744 atoms chosen to match the experimental composition ([C] = 74±3 at.%; [H] = 26±3 at.%, measured by hydrogen forward scattering, Evans Analytical Group, Sunnyvale, CA, USA). The initial density for the a-C:H samples was 2.6 g/cm^3 which was reduced to 2.3 g/cm^3 after relaxation (experimental a-C:H density was 2.1 g/cm^3).

The a-C:H:Si:O samples were annealed at 550, 800, and 1100 K for 60 ps. The temperature was controlled via a Nose-Hoover thermostat and was ramped to the target temperature over 5 ps. For comparison a simulation was also run at 300 K for 60 ps. a-C:H samples were annealed at 800 and 1100 K for 60 ps with the same heating procedure used for the a-C:H:Si:O samples.

Distributions of bond lengths were obtained from MD simulations by computing the fractions of sp^3-hybridized carbon atoms bonded to atom X (where X can be H, C, or Si) and plotting them against the bond length. These distributions of bond length were normalized by the total number of sp^3 C-X bonds (where X is C, H, and Si). This normalization procedure provides physically meaningful insights into the structure of amorphous carbon since the sum of the bars in one of the histograms between two bond lengths (L_1 and L_2) represents the probability of finding in the simulation a sp^3 C atom having a C-X bond with bond length between

L_1 and L_2. The fraction of sp^3 C-C relative to sp^3 C-X is not the same for the a-C:H and a-C:H:Si:O since in the former there are sp^3 C-C and sp^3 C-H bonds, while in the latter there are sp^3 C-C and sp^3 C-H bonds as well as sp^3 C-Si bonds (and the [H] is slightly different in a-C:H:Si:O). Thus, the sum of the bars in the histograms for sp^3 C-C bonds vs. bond length distribution (Figure 2d) is not the same for a-C:H and a-C:H:Si:O.

Distributions of sp^3 C-C bond lengths were also analyzed by setting the area of the histograms shown in Figure 2d equal to 1 (Figure S.7). This normalization procedure provides complementary information to the analysis performed by normalizing the distributions by the total number of sp^3 C-X bonds (where X is C, H, and Si): while the former was used to compute the probability that a randomly selected sp^3 C-C bond has a length between two values (L1 and L2), the latter was used to extract the probability of finding a sp^3 C atom forming a C-C bond with a length between L1 and L2.

Modeling the Structural Evolution of Silicon- and Oxygen-Containing Hydrogenated Amorphous Carbon

Clustering and Ordering of sp^2-Bonded Carbon

To compute the activation energy for the clustering and ordering of sp^2 carbon in a-C:H:Si:O, the ratio of the intensity of the π-π* shake-up satellites to that of the a-C:H:Si:O synthetic peak (this ratio is proportional to the total number of sp^2-bonded carbon atoms in ordered clusters) was plotted as a function of temperature (Figure 1e). The experimental data was fit with a model, which assumes that the clustering and ordering of sp^2 carbon only requires thermal activation over an energy barrier. Because of bond length and angle disorder in amorphous carbon-based materials[35], a distribution of activation energies for the clustering and ordering of sp^2 carbon was introduced. The equation employed to calculate the clustering and ordering of sp^2 carbon as a function of time and temperature is:

$$\frac{C1s_{\pi-\pi^*}}{C1s_{a-C:H:Si:O}}(t,T)=\frac{C1s_{\pi-\pi^*}}{C1s_{a-C:H:Si:O}}(0,RT)+\int N\left(E_a\right)\left[1-\exp\left(\int_0^t -\upsilon_0\exp\left(-\frac{E_a}{k_BT}\right)d\tau\right)\right]dE_a \qquad \text{Eq. 2}$$

where $\frac{C1s_{\pi-\pi^*}}{C1s_{a-C:H:Si:O}}(0,RT)$ is the ratio of the intensity of the π-π*shake-up satellites to that of the a-C:H:Si:O synthetic peak for unannealed a-C:H:Si:O, $N(E_a)$ is the probability distribution versus activation energy (E_a), υ_0 is the attempt frequency typical for solid state reactions (chosen to be 10^{13} s^{-1} [36]), and k_B is Boltzmann's constant. $N(E_a)$ was assumed to be a Gaussian distribution.

The experimental data were fit with Equation 2, using the area, mean and standard deviation of the Gaussian distribution as fitting parameters. The fitting of the present data (Figure 1e) yielded an activation energy distribution for the clustering and ordering of sp^2 carbon in a-C:H:Si:O of 0.22±0.08 eV (correlation coefficient: 0.85).

Conversion of sp^3- to sp^2-Hybridized Carbon

Sullivan *et al.*[36] developed a model for describing the transformation of sp^3 to sp^2-hybridized carbon in ta-C. The model involves an expression for the conversion *vs.* temperature and time under the assumption that rehybridization only requires thermal activation over an energy barrier, *i.e.*, is governed by first order reaction rate theory. Because of bond length and angle disorder in ta-C, Sullivan *et al.* postulated a distribution of activation energies for sp^3-to-sp^2 conversion.

In the present work, the model of Sullivan *et al.* was used to fit the variation of sp^2 fractions with annealing temperature calculated on the basis of NEXAFS spectra (Figure 2). The equation employed to calculate the fraction of sp^2-bonded carbon as a function of time and temperature is:

$$sp^2(t,T)=sp^2(0,RT)+sp^3\left(0,RT\right)\int N\left(E_a\right)\left[1-\exp\left(\int_0^t -\upsilon_0\exp\left(-\frac{E_a}{k_BT}\right)d\tau\right)\right]dE_a \qquad \text{Eq. 3}$$

where $sp^2(0,RT)$ is the fraction of sp^2 carbon for unannealed a-C:H:Si:O, $sp^3(0,RT)$ is the fraction of sp^3 carbon for unannealed a-C:H:Si:O, $N(E_a)$ is the probability distribution of the sp^3 fraction versus activation energy (E_a), υ_0 is the attempt frequency typical for solid state reactions (chosen to be 10^{13} s^{-1} [36]), and k_B is Boltzmann's constant. $N(E_a)$ was assumed to be a Gaussian distribution and was normalized to set its area equal to 1.

The variation of sp^2 fractions *vs.* annealing temperature calculated on the basis of NEXAFS spectra (Figure 3) was fit with Equation 3 using the mean and standard deviation of the Gaussian distribution as fitting parameters. The fitting of the present data (Figure 3c) yielded an activation energy distribution for sp^3-to-sp^2 conversion of 3.0±1.1 eV (correlation coefficient: 0.99).

Importantly, in the case of a-C:H, the model proposed by Sullivan *et al.* could be refined to describe the thermally-induced sp^3-to-sp^2 conversion of carbon[11]. The refined model accounts for the presence of hydrogen in a-C:H through the introduction of a second distribution of activation energies in the expression for the transformation of sp^3 to sp^2 carbon as a function of time and temperature. This refined model could describe the experimental data well[11]. In the case of a-C:H:Si:O, even though the model of Sullivan *et al.* nicely fit the experimental data of the thermally-induced evolution of the carbon bonding configuration, a careful description of the structural evolution of this material would require the introduction of three distributions of activation energies in the expression for the conversion of sp^3 to sp^2 hybridization as a function of time and temperature due to the presence of carbon-carbon, carbon-hydrogen, and carbon-silicon bonds. Fitting the experimental data with such a refined model that includes three distributions of activation energies was avoided since the model would be over-parameterized and require the knowledge of the relative fractions of carbon-carbon, carbon-hydrogen, and carbon-silicon bonds (not available experimentally).

Results

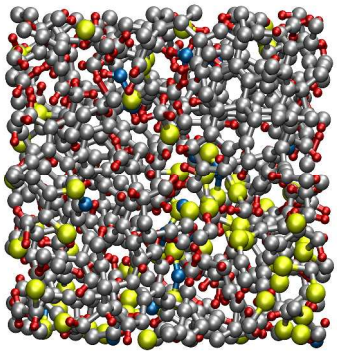

Figure S.1. Representative a-C:H:Si:O structure from MD simulations performed using the ReaxFF potential[28]. The atoms are C (silver), H (red), O (blue), and Si (yellow).

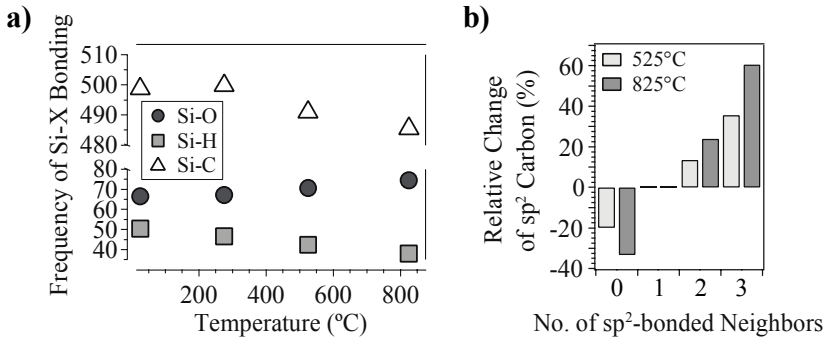

Figure S.2. (a) Frequency of Si-X bonds (where X = O, H, or C) *vs.* annealing temperature calculated from MD simulations performed using the ReaxFF potential[28]. The increase in the frequency of Si-O bonds together with the decrease in the frequency of Si-C and Si-H bonds suggest a progressive increase in the oxidation state of Si, in agreement with XPS results; (b) relative change (relative to the values for the unannealed a-C:H:Si:O structure) in the fraction of sp^2-bonded carbon atoms with different numbers of neighboring sp^2-bonded carbon atoms upon annealing at 525°C and 825°C. Upon providing thermal energy to a-C:H:Si:O, the number of sp^2-hybridized neighbors around each sp^2-bonded carbon atom increases, thus suggesting the progressive clustering of sp^2 carbon atoms (*note*: the variation in the fraction of sp^2-hybridized carbon neighbors upon annealing is much larger than the increase in the fraction of sp^2-bonded carbon upon annealing, see Figure 2 in the main text).

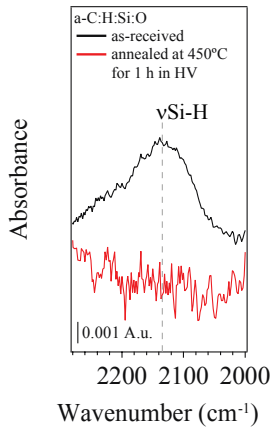

Figure S.3. Attenuated total reflection Fourier-transform infrared (ATR/FT-IR) spectra in the region between 2000 and 2300 cm^{-1} (corresponding to the Si-H stretching vibration[37]) of a-C:H:Si:O before and after annealing at 450°C for 1 h under high vacuum conditions. The decrease in intensity of the absorption peak assigned to the Si-H stretching vibration agrees well with the decrease in the number of Si-H bonds upon annealing observed in MD simulations (Figure 2 and Figure S.2). Experimental details for ATR/FT-IR experiments: ATR/FT-IR spectra were acquired with a Nicolet 8700 Fourier Transform Infrared spectrometer (Thermo Electron Corporation, Madison, WI, USA) equipped with a Seagull^{TM} ATR unit (Harrick Scientific Products, Inc., Pleasantville, NY, USA). ATR/FT-IR spectra were acquired in a spectral range between 4000 and 650 cm^{-1} with a resolution of 4 cm^{-1}. The angle of incidence of the IR beam on the Ge ATR crystal was 45°. The spectra were processed with OMNIC software (V7.2, Thermo Electron Corporation, Madison, WI, USA). A background correction was applied to all experimental spectra using the single beam spectrum of the ATR crystal collected before each experiment. The ATR/FT-IR spectra are reported without any baseline and ATR correction, *i.e.*, as-acquired.

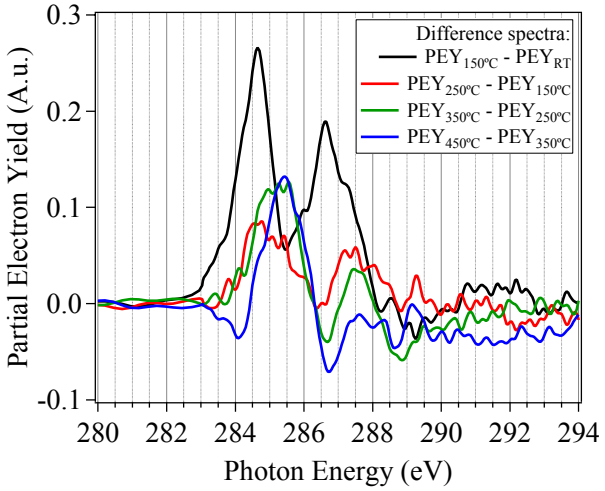

Figure S.4. Difference in the NEXAFS C 1s partial electron yield spectra of a-C:H:Si:O between subsequent annealing steps (*i.e.*, spectrum acquired at annealing step *i* (*PEY*$_i$) minus spectrum acquired at annealing step *i-1* (*PEY*$_{i-1}$)). A positive peak is detected at 285.0-285.5 eV (assigned to the C 1s→π* transition for disordered carbon-carbon bonds[21, 38]) for all annealing steps, which suggests a progressive increase in the fraction of sp^2-bonded carbon in the near-surface region of a-C:H:Si:O upon annealing. The shift to higher photon energy of the peak maximum as the annealing temperature is increased indicates an increase in the degree of ordering of the sp^2 bonds. In addition, a negative peak is observed at ~289 eV (C 1s→ σ* transition for C-Si bonds[39])), which indicates the breakage of carbon-silicon bonds. Furthermore, a positive peak is observed at 287.0 (assigned to the C 1s→σ* transition for C-H bonds[21-22, 40]) for the difference spectrum corresponding to the first annealing step (*i.e.*, spectrum acquired at 150°C minus spectrum acquired at room temperature). This peak becomes negative for subsequent annealing steps (*i.e.*, upon heating at higher temperatures), suggesting the scission of carbon-hydrogen bonds upon annealing.

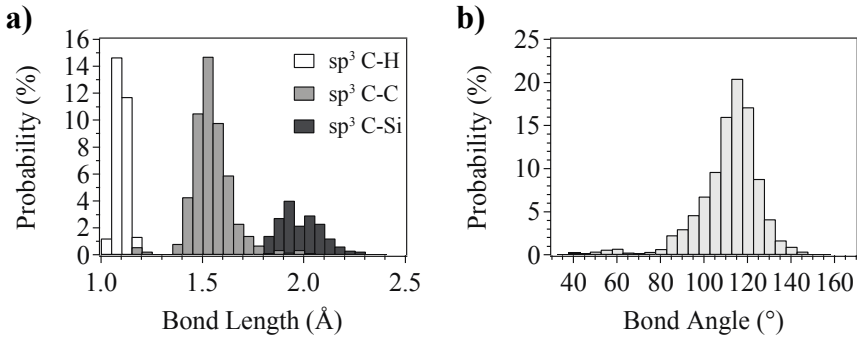

Figure S.5. Distributions of bond lengths (a) and angles (b) for sp^3-hybridized carbon atoms (bonded to H, C, or Si) calculated from MD simulations of a-C:H:Si:O (before annealing) performed using the ReaxFF potential[28]. Due to the presence of only a few carbon-oxygen bonds (<2%), the corresponding distribution of bond lengths is not displayed in (a). The tail in the angle distribution towards smaller bond angles in (b), as well as the small peak at ~60°, is due to the presence of 3- and 4-membered rings, in agreement with previous experimental and theoretical studies of amorphous carbon-based materials[35].

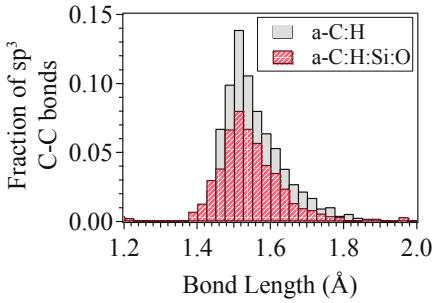

Figure S.6. Fraction of sp^3 carbon-carbon bonds *vs.* bond length for unannealed a-C:H:Si:O and a-C:H. The introduction of silicon in a-C:H results in a narrower distribution of carbon-carbon bonds with less strained bonds due to the greater average bond length of silicon-carbon bonds relative to carbon-carbon bonds (185 pm compared to 154 pm[41]). These distributions of bond length were normalized by the total number of sp^3 C-X bonds (where X is C, H, and Si).

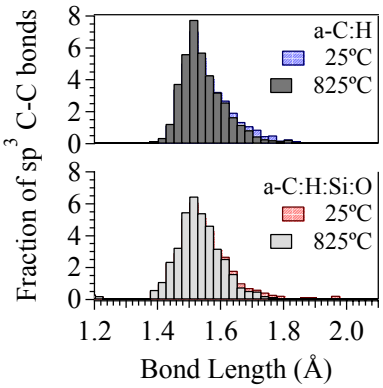

Figure S.7. Fraction of sp^3-hybridized C-C bonds *vs.* bond length for a-C:H:Si:O and a-C:H before and after annealing at 825ºC. The sp^3 C-C bond length distributions were normalized to set their area equal to 1. The introduction of silicon in a-C:H results in a narrower distribution of carbon-carbon bonds with less strained bonds due to the greater average bond length of silicon-carbon bonds relative to carbon-carbon bonds (185 pm compared to 154 pm[41]).

References

1. Kester, D. J.; Brodbeck, C. L.; Singer, I. L.; Kyriakopoulos, A., Sliding wear behavior of diamond-like nanocomposite coatings. *Surface and Coatings Technology* **1999,** *113* (3), 268-273.
2. Neerinck, D.; Persoone, P.; Sercu, M.; Goel, A.; Kester, D.; Bray, D., Diamond-like nanocomposite coatings (a-C:H/a-Si:O) for tribological applications. *Diamond and Related Materials* **1998,** *7* (2-5), 468-471.
3. Neerinck, D.; Persoone, P.; Sercu, M.; Goel, A.; Venkatraman, C.; Kester, D.; Halter, C.; Swab, P.; Bray, D., Diamond-like nanocomposite coatings for low-wear and low-friction applications in humid environments. *Thin Solid Films* **1998,** *317* (1-2), 402-404.
4. Prasad, S. V.; Dugger, M. T.; Christenson, T. R.; Tallant, D. R., LIGA Microsystems: Surface Interactions, Tribology, and Coatings. *Journal of Manufacturing Processes* **2004,** *6* (1), 107-116.
5. Scharf, T. W.; Ohlhausen, J. A.; Tallant, D. R.; Prasad, S. V., Mechanisms of friction in diamondlike nanocomposite coatings. *Journal of Applied Physics* **2007,** *101* (6), 063521-11.
6. Venkatraman, C.; Brodbeck, C.; Lei, R., Tribological properties of diamond-like nanocomposite coatings at high temperatures. *Surface and Coatings Technology* **1999,** *115* (2-3), 215-221.
7. Venkatraman, C.; Goel, A.; Lei, R.; Kester, D.; Outten, C., Electrical properties of diamond-like nanocomposite coatings. *Thin Solid Films* **1997,** *308-309*, 173-177.
8. Venkatraman, C.; Kester, D.; Goel, A.; Bray, D., Diamond-Like Nanocomposite Coatings - A New Class of Materials. In *Surface Modification Technologies IX*, Sudarshan, T. S.; Reitz, W.; Stiglich, J. J., Eds. The Minerals, Metals & Materials Society: **1996**.
9. Koshigan, K. D.; Mangolini, F.; McClimon, J. B.; Vacher, B.; Bec, S.; Carpick, R. W.; Fontaine, J., Understanding the hydrogen and oxygen gas pressure dependence of the tribological properties of silicon oxide–doped hydrogenated amorphous carbon coatings. *Carbon* **2015,** *93*, 851-860.
10. Peng, J.; Sergiienko, A.; Mangolini, F.; Stallworth, P. E.; Greenbaum, S.; Carpick, R. W., Solid state magnetic resonance investigation of the thermally-induced structural evolution of silicon oxide-doped hydrogenated amorphous carbon. *Carbon* **2016,** *105*, 163-175.
11. Mangolini, F.; Rose, F.; Hilbert, J.; Carpick, R. W., Thermally induced evolution of hydrogenated amorphous carbon. *Applied Physics Letters* **2013,** *103* (16), 161605.
12. Mangolini, F.; Ahlund, J.; Wabiszewski, G. E.; Adiga, V. P.; Egberts, P.; Streller, F.; Backlund, K.; Karlsson, P. G.; Wannberg, B.; Carpick, R. W., Angle-resolved environmental X-ray photoelectron spectroscopy: A new laboratory setup for photoemission studies at pressures up to 0.4 Torr. *Review of Scientific Instruments* **2012,** *83* (9), 093112-10.
13. Shirley, D. A., High-Resolution X-Ray Photoemission Spectrum of the Valence Bands of Gold. *Physical Review B (Solid State)* **1972,** *5* (12), 4709-4714.
14. Mangolini, F. Reactivity of Environmentally Compatible Lubricant Additives: An in Situ and Ex Situ Investigation. Swiss Federal Institute of Technology (ETH), PhD Thesis, Zurich, **2011**.
15. Mangolini, F.; Rossi, A.; Spencer, N. D., Chemical Reactivity of Triphenyl Phosphorothionate (TPPT) with Iron: An ATR/FT-IR and XPS Investigation. *The Journal of Physical Chemistry C* **2011,** *115* (4), 1339-1354.
16. Powell, C. J., The Physical Basis for Quantitative Surface Analysis by Auger Electron Spectroscopy and X-ray Photoelectron Spectroscopy. In *Quantitative Surface Analysis of Materials*, McIntyre, N. S., Ed. American Society for Testing and Materials: **1978**, pp 5-30.
17. International, A., Standard Terminology Relating to Surface Analysis. ASTM International: **2003**.
18. Tanuma, S., Electron Attenuation Lengths. In *Surface Analysis by Auger and X-Ray Photoelectron Spectroscopy*, Briggs, D.; Grant, J. T., Eds. IM Publications: Chichester (UK), **2003**; Chapter 11, pp 259-294.
19. Seah, M. P., Quabtification of AES and XPS. In *Practical Surface Analysis*, Briggs, D.; Seah, M. P., Eds. John Wiley & Sons: New York, **1990**, pp 201-255.
20. Fadley, C. S., Solid state—and surface—analysis by means oF angular-dependent x-ray photoelectron spectroscopy. *Progress in Solid State Chemistry* **1976,** *11, Part 3*, 265-343.
21. Stöhr, J., *NEXAFS Spectroscopy*. Springer-Verlag: **1992**; p 403.
22. Mangolini, F.; McClimon, J. B.; Rose, F.; Carpick, R. W., Accounting for nanometer-thick adventitious carbon contamination in X-ray absorption spectra of carbon-based materials. *Anal Chem* **2014,** *86* (24), 12258-65.
23. Mangolini, F.; McClimon, J. B.; Carpick, R. W., Quantitative Evaluation of the Carbon Hybridization State by Near Edge X-ray Absorption Fine Structure Spectroscopy. *Anal Chem* **2016,** *88* (5), 2817-24.
24. Kulkarni, A. D.; Truhlar, D. G.; Goverapet Srinivasan, S.; van Duin, A. C. T.; Norman, P.; Schwartzentruber, T. E., Oxygen Interactions with Silica Surfaces: Coupled Cluster and Density Functional Investigation and the Development of a New ReaxFF Potential. *The Journal of Physical Chemistry C* **2012,** *117* (1), 258-269.
25. Liang, T.; Shin, Y. K.; Cheng, Y.-T.; Yilmaz, D. E.; Vishnu, K. G.; Verners, O.; Zou, C.; Phillpot, S. R.; Sinnott, S. B.; van Duin, A. C. T., Reactive Potentials for Advanced Atomistic Simulations. *Annual Review of Materials Research* **2013,** *43* (1), 109-129.
26. Newsome, D. A.; Sengupta, D.; Foroutan, H.; Russo, M. F.; van Duin, A. C. T., Oxidation of Silicon Carbide by O2 and H2O: A ReaxFF Reactive Molecular Dynamics Study, Part I. *The Journal of Physical Chemistry C* **2012,** *116* (30), 16111-16121.
27. van Duin, A. C. T.; Strachan, A.; Stewman, S.; Zhang, Q.; Xu, X.; Goddard, W. A., ReaxFFSiO Reactive Force Field for Silicon and Silicon Oxide Systems. *The Journal of Physical Chemistry A* **2003,** *107* (19), 3803-3811.
28. van Duin, A. C. T.; Dasgupta, S.; Lorant, F.; Goddard, W. A., ReaxFF: A Reactive Force Field for Hydrocarbons. *The Journal of Physical Chemistry A* **2001,** *105* (41), 9396-9409.
29. Aktulga, H. M.; Fogarty, J. C.; Pandit, S. A.; Grama, A. Y., Parallel reactive molecular dynamics: Numerical methods and algorithmic techniques. *Parallel Comput.* **2012,** *38* (4-5), 245-259.

30. Plimpton, S., Fast Parallel Algorithms for Short-Range Molecular Dynamics. *Journal of Computational Physics* **1995,** *117* (1), 1-19.
31. Li, L.; Xu, M.; Song, W.; Ovcharenko, A.; Zhang, G.; Jia, D., The effect of empirical potential functions on modeling of amorphous carbon using molecular dynamics method. *Applied Surface Science* **2013,** *286*, 287-297.
32. Marks, N. A., Evidence for subpicosecond thermal spikes in the formation of tetrahedral amorphous carbon. *Physical Review B* **1997,** *56* (5), 2441-2446.
33. de Tomas, C.; Suarez-Martinez, I.; Marks, N. A., Graphitization of amorphous carbons: A comparative study of interatomic potentials. *Carbon* **2016,** *109*, 681-693.
34. Marks, N. A., Amorphous Carbon and Related Materials. In *Computer-Based Modeling of Novel Carbon Systems and Their Properties: Beyond Nanotubes*, Colombo, L.; Fasolino, A., Eds. Springer Netherlands: Dordrecht, **2010**, pp 129-169.
35. Robertson, J., Diamond-like amorphous carbon. *Materials Science and Engineering: R: Reports* **2002,** *37* (4-6), 129-281.
36. Sullivan, J. P.; Friedmann, T.; Baca, A., Stress relaxation and thermal evolution of film properties in amorphous carbon. *Journal of Electronic Materials* **1997,** *26* (9), 1021-1029.
37. Socrates, G., *Infrared and Raman Characteristic Group Frequencies*. 3rd ed.; Johk Wiley & Sons: Chichester, **2001**; p 347.
38. Comelli, G.; Stöhr, J.; Robinson, C. J.; Jark, W., Structural studies of argon-sputtered amorphous carbon films by means of extended x-ray-absorption fine structure. *Physical Review B* **1988,** *38* (11), 7511-7519.
39. Wada, A.; Ogaki, T.; Niibe, M.; Tagawa, M.; Saitoh, H.; Kanda, K.; Ito, H., Local structural analysis of a-SiC_X:H films formed by decomposition of tetramethylsilane in microwave discharge flow of Ar. *Diamond and Related Materials* **2011,** *20* (3), 364-367.
40. Sumant, A. V.; Gilbert, P. U. P. A.; Grierson, D. S.; Konicek, A. R.; Abrecht, M.; Butler, J. E.; Feygelson, T.; Rotter, S. S.; Carpick, R. W., Surface composition, bonding, and morphology in the nucleation and growth of ultra-thin, high quality nanocrystalline diamond films. *Diamond and Related Materials* **2007,** *16* (4-7), 718-724.
41. Lide, D. R., *The CRC Handbook of Chemistry and Physics*. CRC Press: Cleveland, Ohio, USA, **2004**; p 2565.